

Evaluation of the E614 Chamber Performance

A Report for the E614 Collaboration Meeting of April 24, 1998

Maher Quraan

April 10, 1998

TRIUMF

Contents

1	Introduction	2
2	Calibrations	2
2.1	Drift Distance	2
2.2	TDC Time Zero	4
3	Cuts	5
4	Timing and Drift Characteristics	5
4.1	TDC Time, Width, and Ionization Clusters	5
4.1.1	Minimum Ionizing Particles	5
4.1.2	Highly Ionizing Particles	7
4.2	Drift Distance	7
5	Tracking	12
5.1	Tracking Method	12
5.2	Chamber Resolution	13
5.3	Plane and Wire Positions	15
5.4	Plane Rotations	17
5.5	Tracking Method When Multiple TDC hits are Present	19
5.6	Tracking Method When Cross Talk Hits are Present	20
6	Efficiency	20
6.1	High Voltage and Threshold Dependence	20
6.2	Drift Distance Dependence	21
6.3	Wire to Wire Variations	21
6.4	Intensity Dependence	24
7	Noise and Cross Talk	24
7.1	Noise	24
7.2	Cross Talk for Minimum Ionizing Particles	26
7.3	Cross Talk for Highly Ionizing Particles	26
8	Improved Calibrations	30
8.1	Finding TDC Time Zero	30
8.2	Finding the Wire Positions	30
8.3	Fine Tuning the GARFIELD File	33
8.4	The BIG Iteration	33
9	Conclusions	33

1 Introduction

Analysis is presently underway for the test run data acquired in August, 1997. This test run was aimed at studying the efficiency and tracking precision of seven proportional drift chambers (PDCs), to arrive at conclusions regarding the design, construction, and assembly of the E614 chamber. No field wires were used in this test assembly. The seven PDCs were assembled such that the two outer PDCs measure the y-position (vertical), whereas the inner five PDCs measure the x-position (horizontal). Wires in each plane are 4 mm apart, with a 2 mm separation from the cathode planes. DME gas was used to fill all chambers. Two scintillators, placed behind the PDC assembly, provided a common stop for the wire TDC's. The TRIUMF M13 beam line provided a beam of pions at $p = 150$ MeV/c (minimum ionizing) and a beam of muons at $p = 30$ MeV/c (highly ionizing).

The method used in analyzing the test data is presented here, as well as the results obtained. Conclusions from this analysis are also presented.

2 Calibrations

The chamber calibrations require the following:

1. A calibration for the drift distance as a function of drift time.
2. Determination of the TDC time zero for each wire.
3. Determination of the wire positions.

Since the first two calibrations are required before proceeding with the analysis, they are discussed in this section. Determining the wire positions, on the other hand, requires tracking information and is therefore discussed in the tracking section.

2.1 Drift Distance

There are two methods to obtain a calibration for the drift distance as a function of TDC time:

1. Using the data itself to obtain this calibration by assuming that the integral of the TDC spectrum is proportional to the drift distance.
2. Using GARFIELD to obtain the calibration, which requires supplying GARFIELD with all the details about the chamber.

The assumption that the drift distance is proportional to the integral of the TDC spectrum follows from the following argument. For tracks traversing the cell at 0° the

number of hits arriving from a strip of the cell of thickness dx is dN , such that

$$dN(x) = ndx, \quad (1)$$

where n is the number density of tracks across the cell (which is a constant if we assume the tracks are equally distributed through the cell). We then have

$$dN(t) = nv_d(t)dt, \quad (2)$$

where v_d is the drift velocity of the electrons. The quantity $dN(t)/dt$, therefore, corresponds to our TDC spectrum, where dt is the TDC channel width. The drift distance $d(t)$ for electrons arriving from a distance with coordinates (t, x) at a wire with coordinates (t_w, x_w) is then given by

$$d(t) = \int_{t_w}^t v_d(t')dt' \propto \int_{t_w}^t \frac{dN(t')}{dt'}dt', \quad (3)$$

and is therefore proportional to the integral of the TDC spectrum, provided that n is a constant.

Since the field around the wires is not spherically symmetric, tracks traversing the detector at different angles will result in TDC spectra with different shapes. The drift distance $d(t)$ is therefore a function of the track angle as well as time, $d = d(t, \theta_t)$. If the data is used to obtain a drift distance calibration, it is necessary to bin the data in angle, with a bin size that is as fine as is required to obtain the desired resolution).

GARFIELD, on the other hand, generates a detailed mapping of the field inside the wire cell (provided that all relevant information is correctly supplied to GARFIELD). Figure 1 shows the drift distance as a function of TDC time as obtained from GARFIELD. Different calibration files are obtained for runs at different high voltages and chamber orientation. Since no pressure or temperature measurements have been obtained in our test run, we assume that $T = 20^\circ C$ and $P = 1 atm$. While this provides a good starting point, a detailed understanding of GARFIELD is desired to improve on the accuracy of this calibration, including discriminator threshold effects and sensitivity to pressure, temperature, gas mixture and track angle. It is also worth noting that if the first calibration method is used (i.e. integrating the TDC spectrum instead of using GARFIELD), it may serve as a starting point, followed by several iterations (using tracking information) to fine-tune the calibration file. However, this iteration may also be done if we start with GARFIELD, with the added advantage that starting with GARFIELD will cut down on the number of iterations required. This iteration may not be required at all, however, if we are satisfied that GARFIELD is providing us with a sufficient calibration.

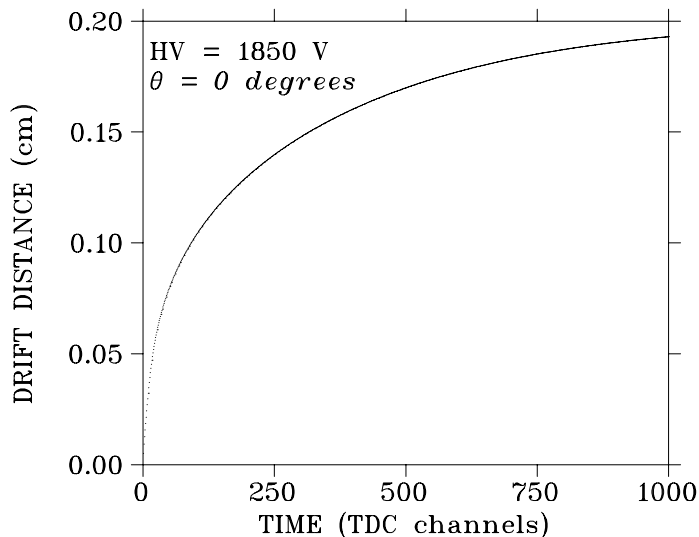


Figure 1: Drift distance as a function of TDC time as obtained from GARFIELD for the X planes at a high voltage of 1850 V.

We currently propose generating a 2-d matrix for the drift distance R_d as a function of the angle of the track θ_t and the (TDC) time t , $R_d(\theta_t, t)$, with a time bin width of 1 TDC channel ($0.5ns$) and a θ_t bin width comparable to our θ_t resolution ($\sim 0.5^\circ$).

2.2 TDC Time Zero

A determination of TDC time zero (T_0) is required for each wire in the chamber. A possible method for doing this is to start by finding the peak N_p of the TDC spectrum and assuming that T_0 is the TDC time corresponding to fN_p , where f is some fraction (chosen to give a good starting point). This may be followed by an iteration to fine tune the value of T_0 using tracking information. For the time being, a plane-by-plane T_0 is determined from the TDC spectrum of the individual planes for each run. The variations of T_0 from wire to wire within the same plane in this test run is small, however, a dependence on high voltage is evident. As will be seen in the tracking section the level of accuracy in the tracking residuals confirms that the values used for T_0 are reasonably accurate.

3 Cuts

Various cuts have been investigated in this analysis. The global cuts imposed were the following:

1. Events with only one hit in the small scintillator are accepted.
2. Events with only one hit in the large scintillator were accepted. However, this requirement was not imposed on runs (159-164), as the the signal from the large scintillator was plugged in the TDC ground channel for those runs!
3. The number of X planes firing was required to exceed a certain value. When resolutions are investigated, 5/5 X planes are required to fire. This is done to ensure that there are enough hits to result in a reasonable track reconstruction. When efficiencies are calculated this requirement is reduced to 2/5 X planes to avoid a correlation that might bias the efficiency.

In addition to these global cuts, other cuts have been imposed in the tracking code:

1. Hits with a TDC time smaller than T_0 or greater than the maximum TDC channel obtained from GARFIELD are not used in the track reconstruction.
3. Since the GARFIELD file is calculated assuming a tracking angle $\theta_t = 0^\circ$, the tracking residuals shown here are only plotted for events with a tracking angle $-1^\circ < \theta_t < 1^\circ$. A complete GARFIELD calibration file, as well as estimates of GARFIELD's sensitivity to tracking angle (which is a function of tracking angle!) are still required.

4 Timing and Drift Characteristics

4.1 TDC Time, Width, and Ionization Clusters

4.1.1 Minimum Ionizing Particles

The TDC arrival time is shown in figure 2 for the five X planes. Figure 3 shows the correlation between the signal arrival time on the sense wire and the signal width. The circuit used in the old front end served to shape the signal resulting in a generally fixed width around 500 TDC channels. This may be clearly seen from the top plots of figure 3 which were obtained with this circuit. This circuit was altered in the new front end so that no signal shaping was done. This allows us to see the real signal width and, therefore, observe the correlation between the signal width and arrival time, as well as observing the individual clusters generated at different points along the track as the particle traverses the cell.

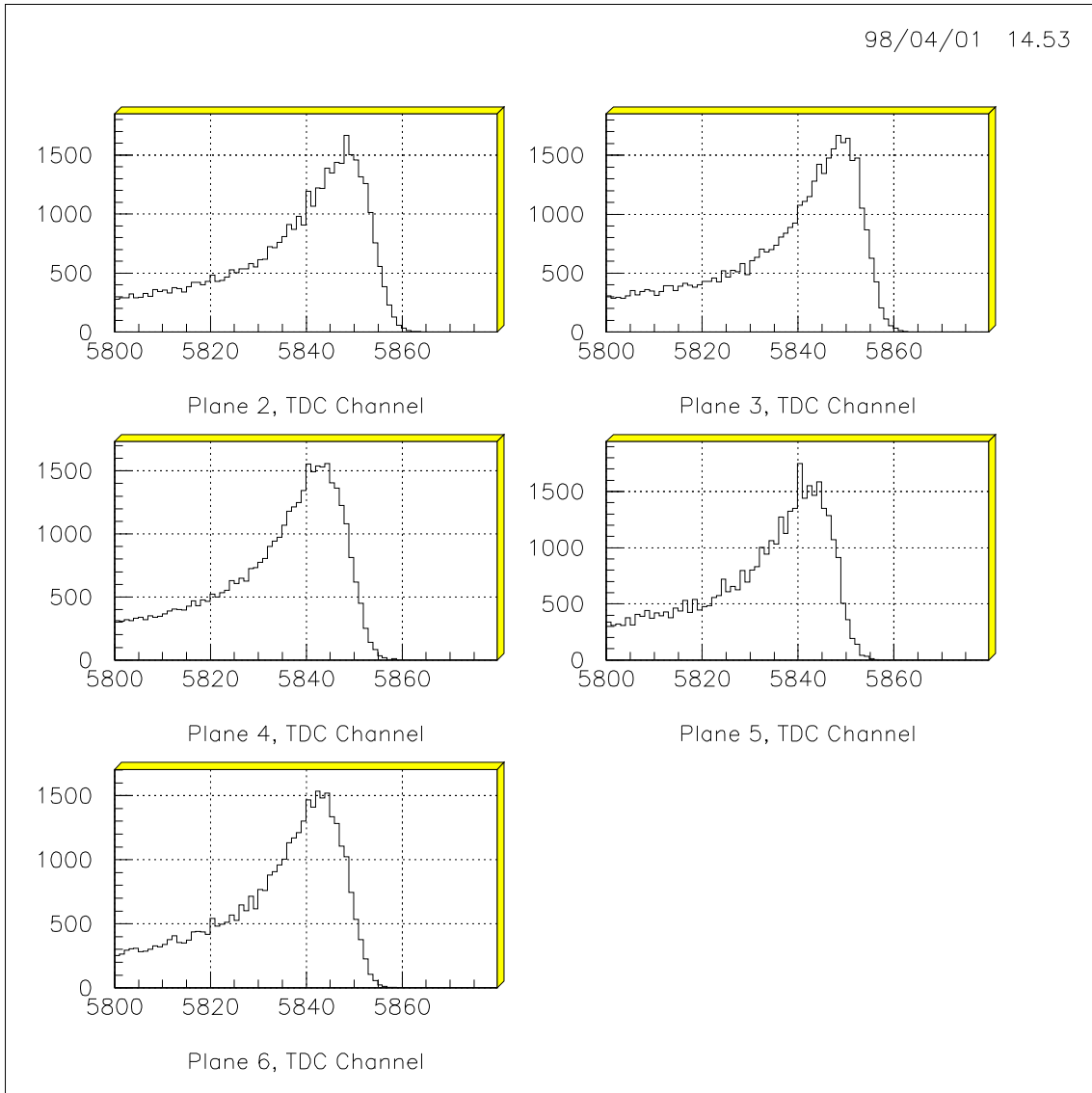


Figure 2: TDC spectra for the X planes from run 170 acquired at a high voltage of 1850 V with the new front end at a threshold of 140 mV.

A cut at 50 TDC channels was initially imposed on the TDC signal width to reduce noise. For data obtained with the new front end, this cut was shown to cut out some of the good hits and, therefore, reduce the efficiency. **It was concluded that no such cut should be used, as there is no clear distinction between good hits and noise based on the TDC signal width with the new front end.** Figure 4 shows the TDC channel multiplicity for data obtained with the old front end, and the new front end at two different thresholds. The old front end shows less TDC channel multiplicities since the long fixed width circuit does not allow us to see the individual clusters; and only the TDC signal that arrives first is registered in most cases. The histograms shown in figure 4 were obtained requiring a TDC signal width > 50 TDC channels. When this cut is removed the average hit multiplicity for the new front end data increases such that $\sim 30\%$ of the events have more than 1 hit/channel. This ratio increase to 47% for the μ runs. Choosing the correct TDC hit was done using tracking information and will be discussed in the tracking section.

4.1.2 Highly Ionizing Particles

Figure 5 shows the signal width versus arrival time for data acquired with a μ -beam with the new front end. While the shape of this spectrum is not understood, the width of the TDC signal for muons is much longer than that for pions. This is to be expected, since the μ -beam is highly ionizing, and more clusters are generated along the particle's track. In the actual E614 experiment, the long width of the TDC muon signal might result in loosing positron signals from these cells, and signal shaping may have to be considered.

4.2 Drift Distance

Once a calibration file is obtained from GARFIELD, the TDC arrival time may be translated into a drift distance. Figure 6 shows the drift radius of the five X planes obtained from the TDC arrival time of figure 2 using the GARFIELD mapping of figure 1. The histograms for the different planes look similar as expected. This drift distance R_d is the minimum distance between the track and the wire and is used to construct a circle around the hit wire. The tracking code provides means to find the correct point on this circle (i.e. a ϕ coordinate) where the hit occurred, as described below.

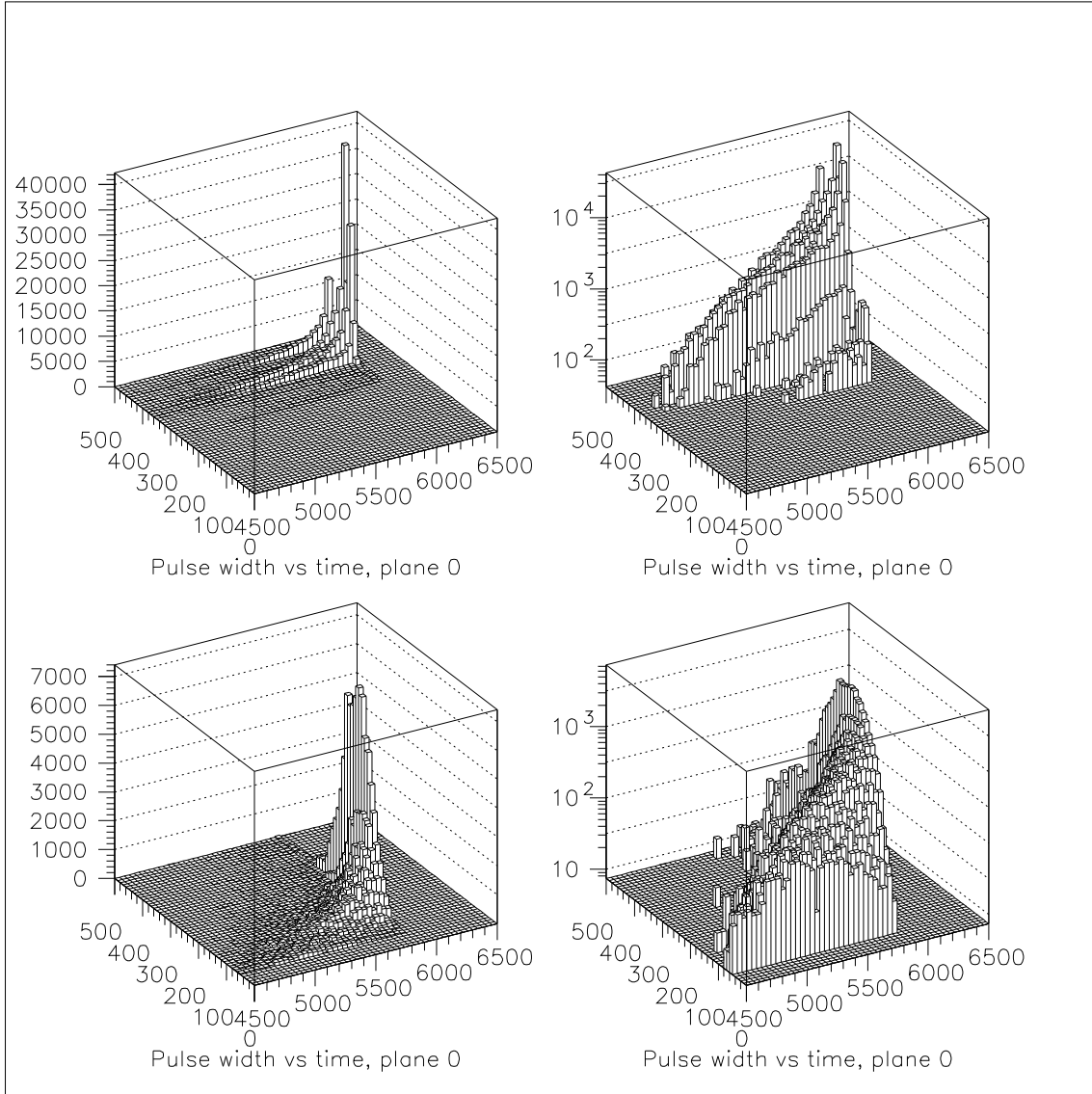


Figure 3: TDC timing width vs arrival time for run 90 (top plots), and run 159 (bottom plots). Both runs were obtained at a high voltage of 1850V and a chamber orientation of 0° . Run 90, was obtained with the old front end while run 159 was obtained with the new front end. A cut was imposed on both histograms so that hits with a TDC width < 50 TDC channels were rejected. All data is from π -beam runs

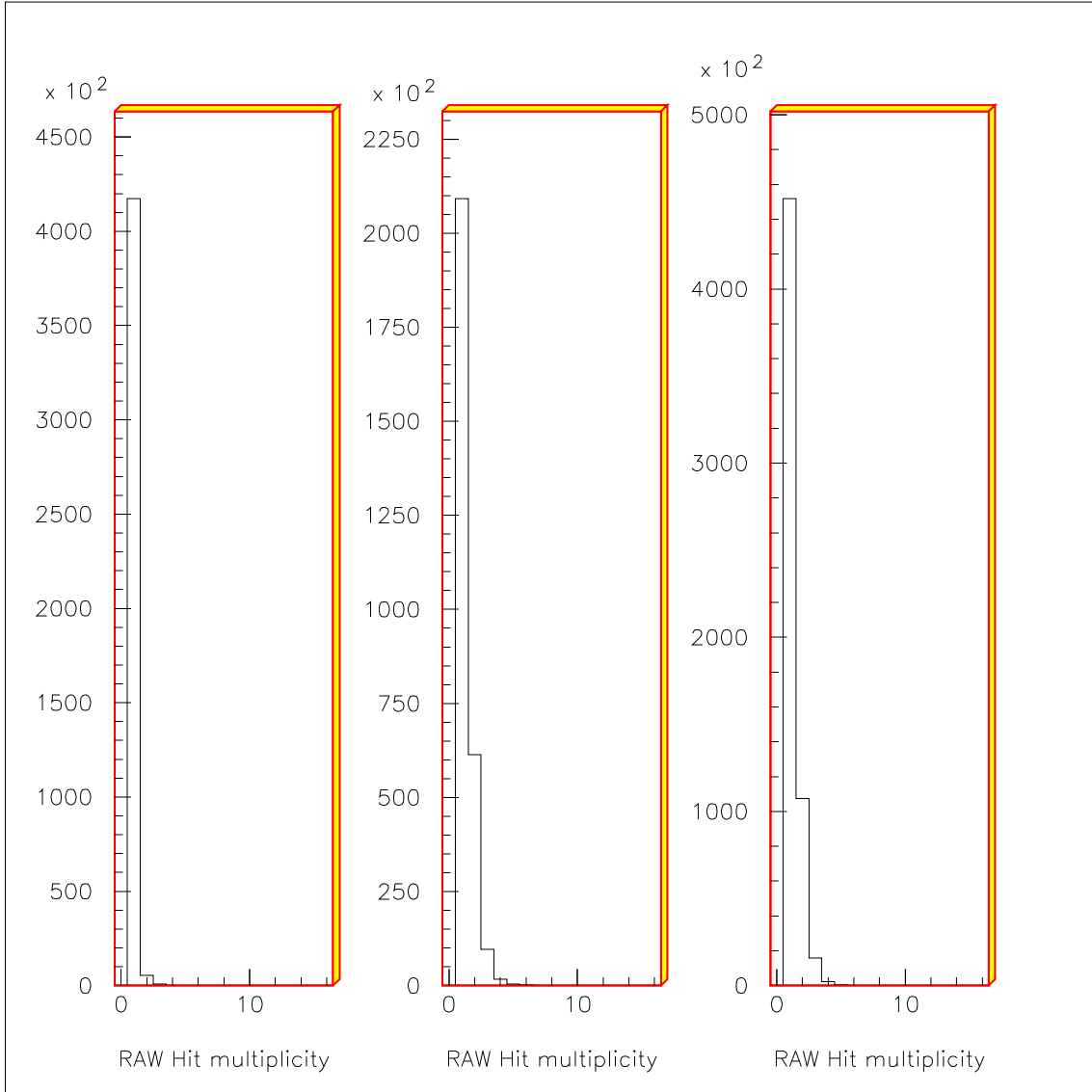


Figure 4: TDC channel multiplicity for data obtained with (a) the old front end at a 200 mV front end threshold, (b) the new front end at a front end threshold of 220 mV, and (c) the new front end at a front end threshold of 140 mV. All these runs were performed at a high voltage of 1850V and a chamber orientation of 0° .

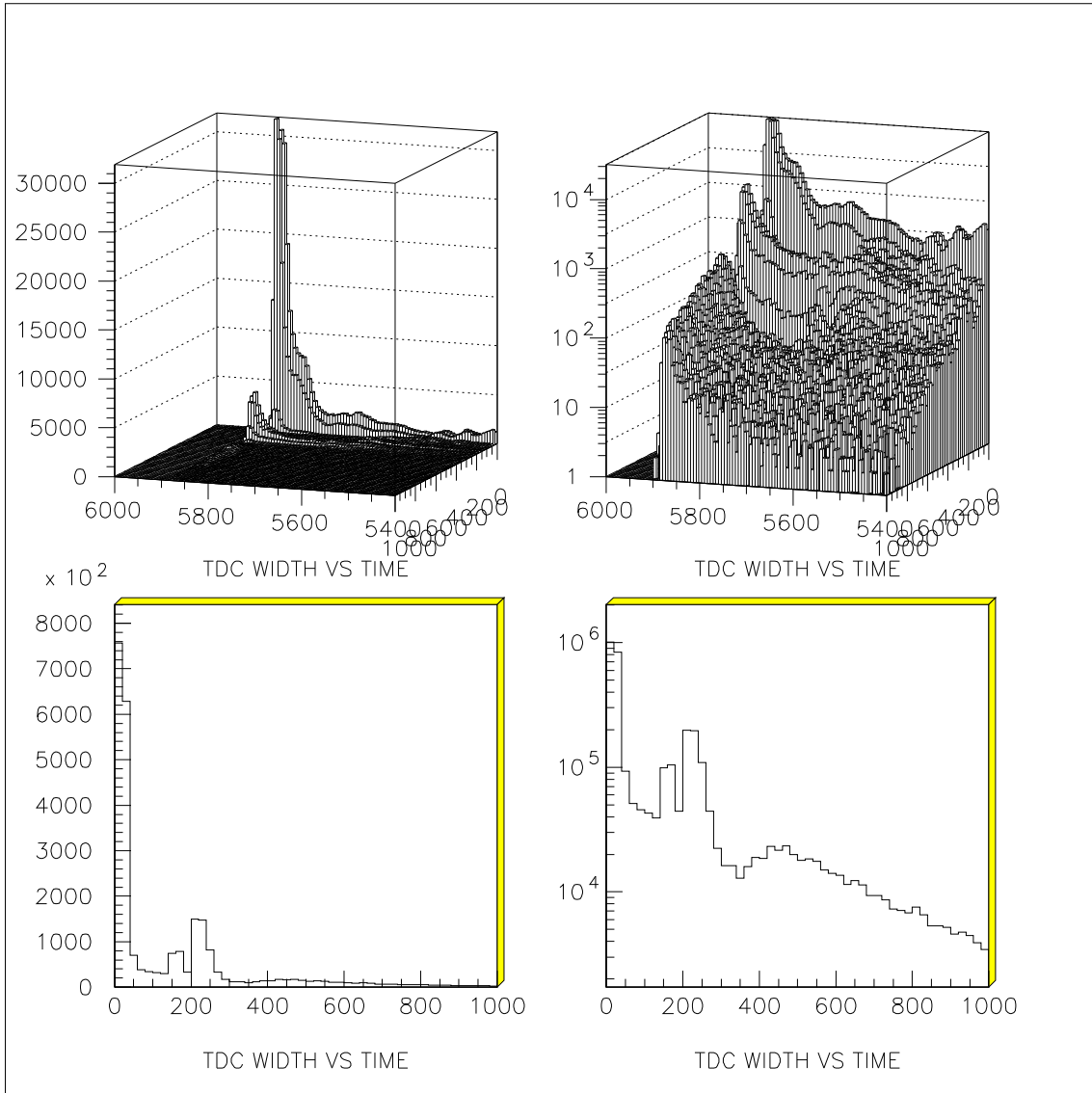


Figure 5: TDC timing width vs arrival time for μ data acquired with the new front end. The top plots are shown on a linear scale (left) and a logarithmic scale (right). The bottom plots are y-projections of the top plots to show the distributions in terms of TDC width.

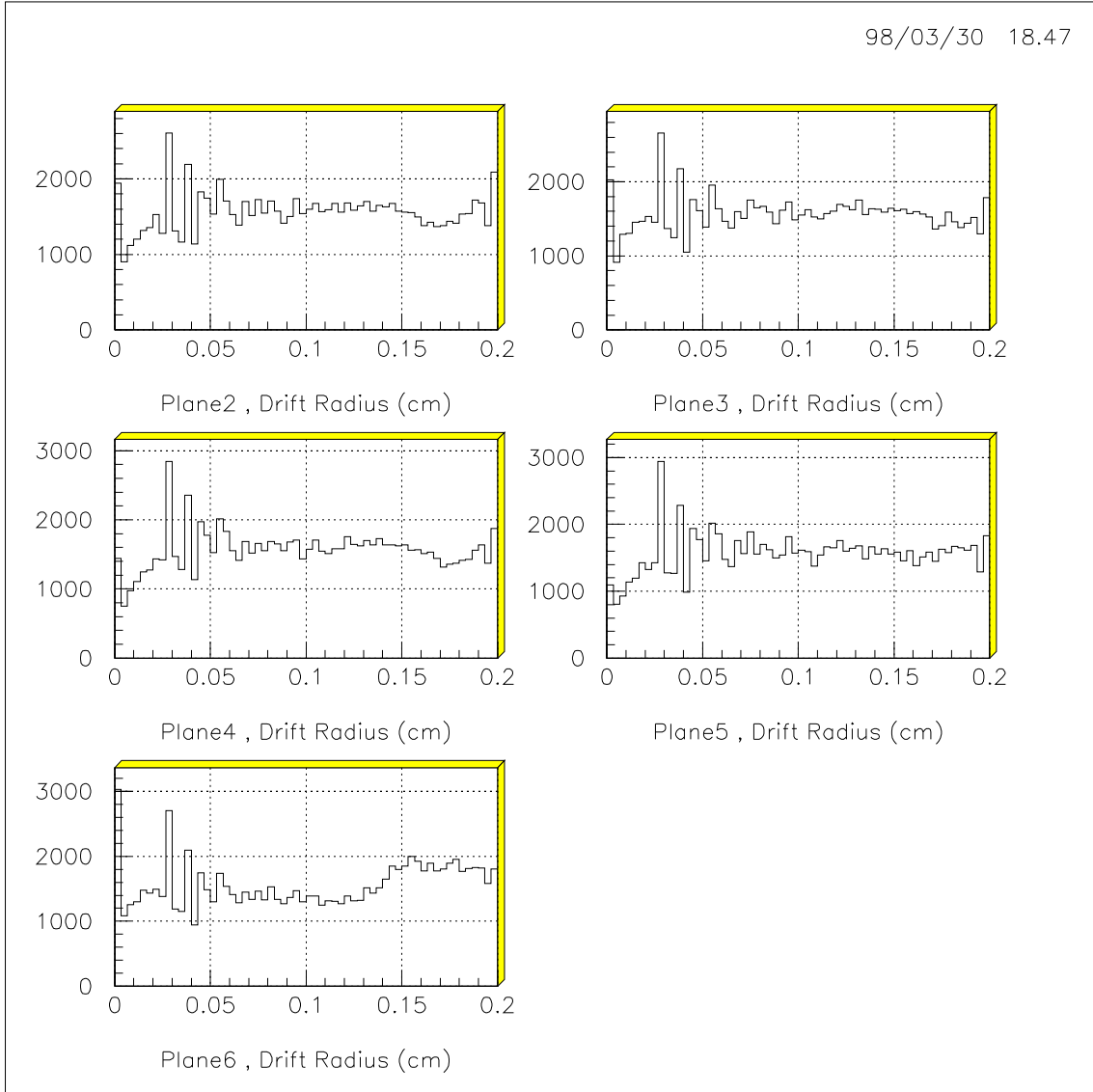
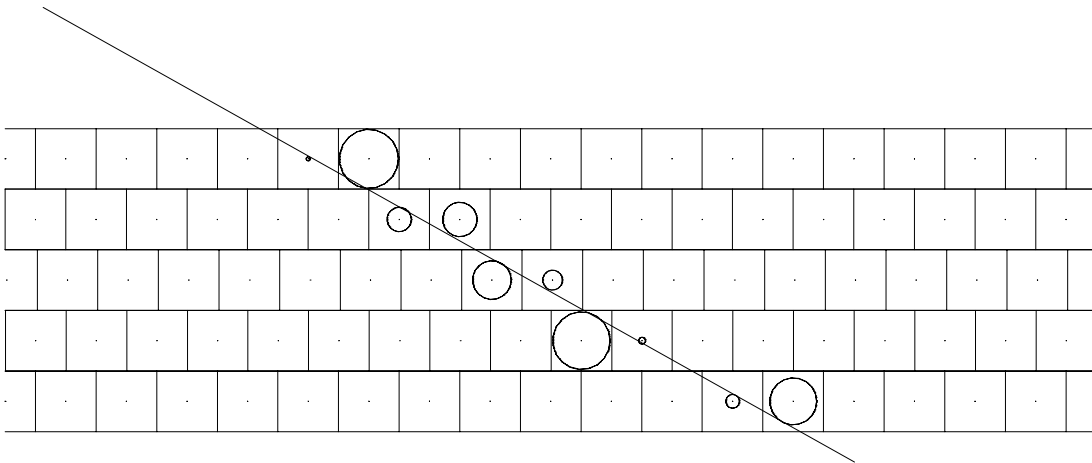


Figure 6: Drift distance histograms calculated for the X planes from run 170 acquired at a high voltage of 1850 V with the new front end at a threshold of 140 mV.



RUN 123
EVENT 53

Figure 7: Schematic view of a typical pion track fitted to the drift circles in the chamber’s X planes.

5 Tracking

5.1 Tracking Method

Figure 7 is a schematic view of a pion track fitted to the drift circles in the X planes. The tracking process starts by fitting a track using wire positions (no timing). This allows an initial estimate of the angle of the track θ_i^t , which is then used to find the hit position on each drift circle such that the track is tangent to the circle. The hit position in the detector’s coordinate system is described by

$$\begin{aligned} x_h &= x_w + R_d \cos(\phi_d) \\ z_h &= z_w + R_d \sin(\phi_d) \end{aligned} \tag{4}$$

where (R_d, ϕ_d) are the hit coordinates relative to the wire. Since there are two points on each drift circle that the track could be tangent to (corresponding to the “left”/”right” side of the circle), a tracking residual (defined as the distance of closest approach between the track and the hit) for both points are computed and the hit corresponding to the smaller residual is chosen as the correct hit. Once the hit position is determined for all the hits, the track fitting process is repeated and a new angle θ^t is obtained. The new angle is used again to re-determine the hit position on the drift circle, and the same steps are repeated. This iteration process continues until the the angle of the track θ^t converges to its “correct” value θ_f^t .

In this present run, the beam makes a specific angle with respect to the chamber, so for a given run the angle is known (to within $\pm 5^\circ$). The method described above, however, does not require a prior knowledge of the angle of the track. Furthermore, this method

allows for a re-determination of the drift radius R_d at each turn in the iteration process, which will be necessary if the angle of the track changes enough to cause $R_d(t)$ to change (since R_d is a function of both time and angle).

5.2 Chamber Resolution

Once a track is constructed, a tracking residual δd (defined as the distance of closest approach between the hit position and the track) is calculated. An average tracking residual δd_{ave} defined by

$$\delta d_{ave} = \frac{1}{N} \sum_{i=1}^N \delta d_i \quad (5)$$

is also calculated, where N is the total number of points used in the fit. Figure 8 shows a histogram of the tracking residuals, δd , and the average tracking residuals, δd_{ave} , obtained from the fit for data acquired at 1850 V and a chamber orientation of 0° . The width of the tracking residuals reflect the intrinsic resolution of the chamber as well as all other factors that may contribute to inaccuracies in the tracking. This includes all the ingredients in equation 5: wire positions, drift distance (where both uncertainties in T_0 and the GARFIELD calibration file contribute). In addition, it reflects any biases in the fitting process, as well as the weighting used in the fit. The reasonably narrow width obtained and the level of symmetry of this histogram provides reasonable confidence in all these factors.

The tracking resolution of the chamber may be determined from the width of the tracking residuals. However, the resolution has a strong dependence on drift distance. The widths of the tracking residuals were determined in 10 bins across the cell (200 μm wide). Since the tracking residuals themselves are dependent on the accuracy of the fit and, therefore, on the weighting of the fit (which is in turn dependent on what we assume the chamber resolutions are as a function of the drift radius), an iterative process is required. After each turn in this iteration, the widths of the 10 tracking residual histograms were determined, fitted to an eight-parameter polynomial and the results are used to weight the fit. A total of 22 iterations were required for this process to converge, after which the resolutions were changing by $< 0.1 \mu m$. Figure 9 shows the result. The chamber resolution improves as a function of drift radius due to the increase in ionization statistics. This general result is independent of gas type, although DME provides high ionization compared to other gases and, therefore, both a more steep increase in the resolution as a function of drift radius and a higher overall resolution. While our result is generally consistent

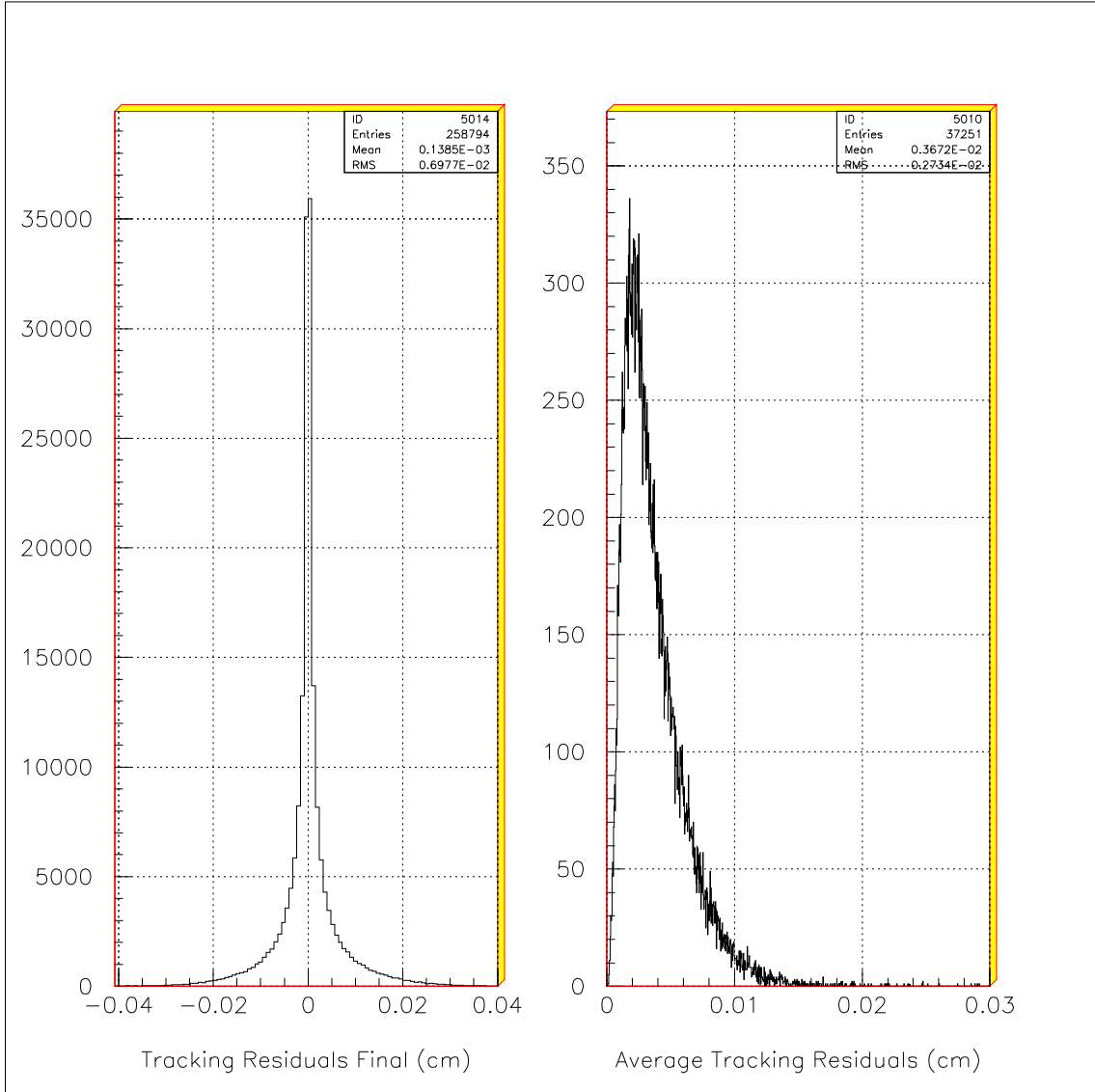


Figure 8: Tracking residuals (for each hit) and average tracking residuals (per event) for data acquired at a high voltage of 1850V and a chamber orientation of 0°.

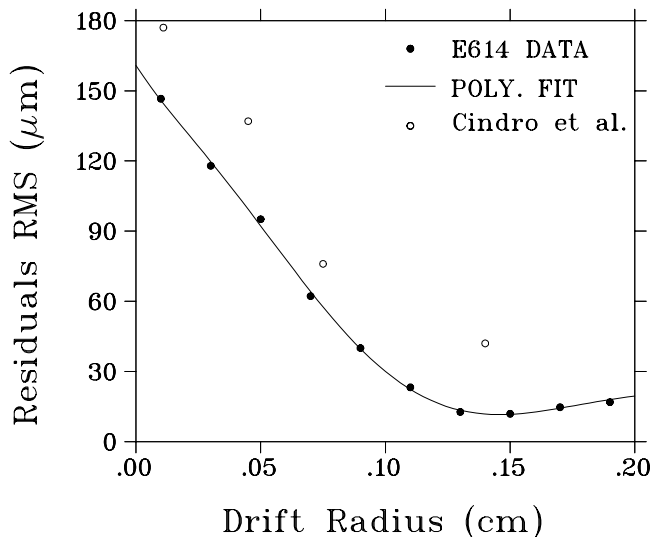


Figure 9: Chamber resolution as a function of drift radius. The dots are computed from data acquired at 1850 V and a chamber orientation of 0^0 ; the curve is an eight-parameter polynomial fit to the data. The circles are data from Cindro et al. obtained with a drift chamber that has a cell size of $10.4 \text{ mm} \times 11.4 \text{ mm}$ and filled with pure DME gas.

with other experiments the minimum resolution obtained (which occurs near $0.15 \mu\text{m}$) is about $12 \mu\text{m}$ in our experiment compared to $30 \mu\text{m}$ for the other experiments. However, as mentioned above, the widths of the tracking residuals (from which these resolutions are determined) reflect on the accuracy of the calibrations, tracking method etc., all of which might have contributed to the lower resolutions obtained in these other experiments (for example inaccuracies in wire positions would smear out the total residuals).

5.3 Plane and Wire Positions

One important and interesting outcome of the results obtained for the chamber resolution is that if we only use hits for which $R_d > 0.12 \mu\text{m}$, a very high resolution may be obtained from the tracking residuals. This very high resolution allows us to determine the plane and wire positions to a very high degree of accuracy ($< 10 \mu\text{m}$). This procedure was used to determine the plane positions yielding the results shown in figure 11 for the plane shifts. Figure 10 shows the tracking residuals for each of the five X planes after these shifts are included in the analysis. Only residuals for which $R_d > 0.12 \mu\text{m}$ are plotted. Figure 12 shows the the tracking residuals when plane 4 is not shifted and excluded from the fit.

The chamber resolution shown in figure 9 is computed from the tracking residuals of

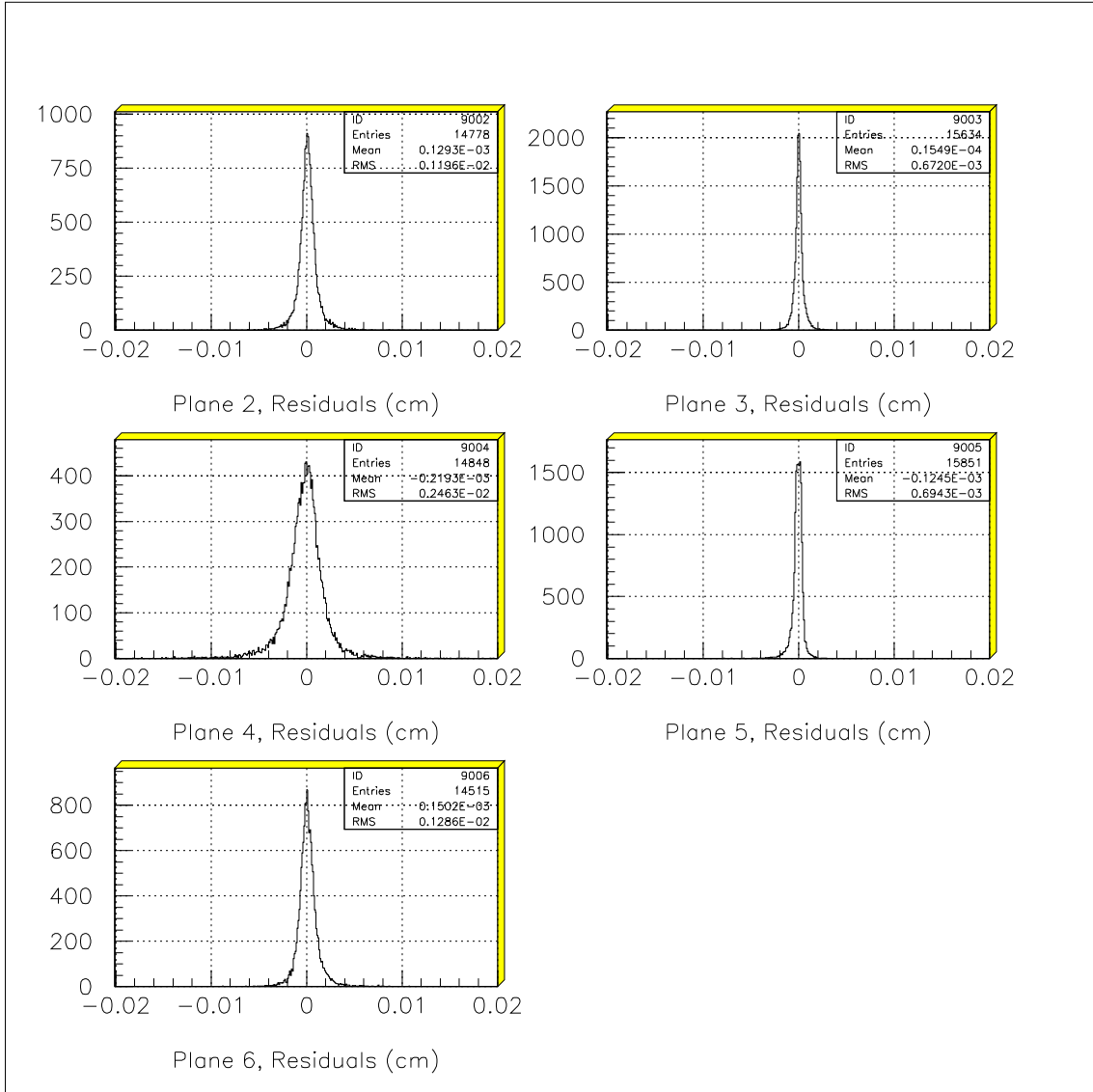


Figure 10: Tracking residuals for each of the five X planes, computed from data acquired at 1850 V with a chamber orientation of 0^0 . The plots were obtained after the appropriate plane shifts were introduced.

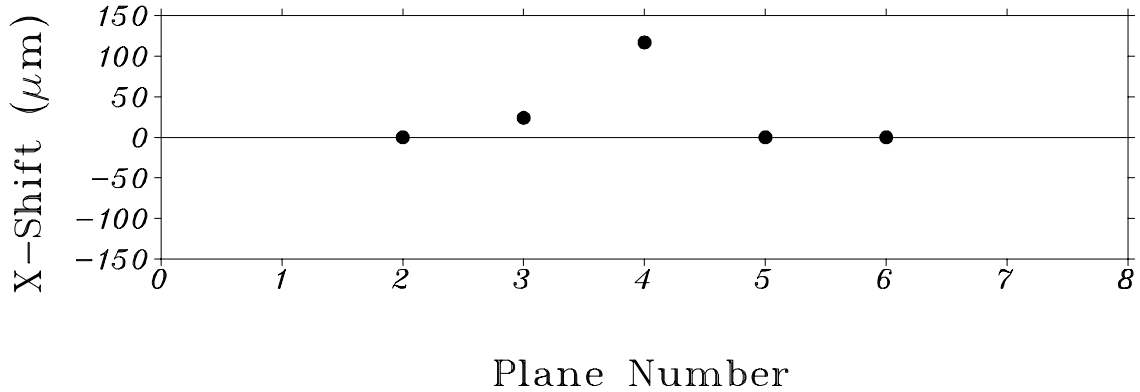


Figure 11: Actual position of the X planes as deduced from tracking.

hits in all wires and in all planes. They, therefore, reflect the accuracy of wire positions. For example each tracking residual histogram in figure 8 is summed over all the wires in that plane and its width, therefore, reflects (in addition to other factors) the scatter of the wires in that plane relative to their assumed positions. A narrow width is only possible if the wires are accurately positioned. An accurate determination of the wire positions, however, maybe achieved through an iterative process as discussed in the last section.

While a shift in the position of a few wires may be observed and corrected for in the software, it is important to emphasize, that a large number of shifted wires or planes may be hard to account for. The tracks, which are used to find these shifts, are themselves determined from the wire positions. If a large number of wires are shifted, a long iteration process becomes necessary to find these shifts. This would also increase the ambiguity in determining other factors such as T_0 and the accuracy of the $R_d(t, \theta)$ calibration file as all these factors are built into the tracking, and may even make these factors quite hard to un-tangle.

5.4 Plane Rotations

A shift in the tracking residuals of a plane (or wire) might be a result of a rotation of that plane (or wire) rather than a shift. If, for example, plane 4 was rotated around the z-axis, this rotation might mimic an x-shift in the tracking residuals. Due to the relatively big shift in plane 4, a test was done to verify that this plane was x-shifted rather than rotated. This was done to reflect on the accuracy construction/assembly process. The Y plane information was used for this purpose; the tracking residuals of the x-planes were

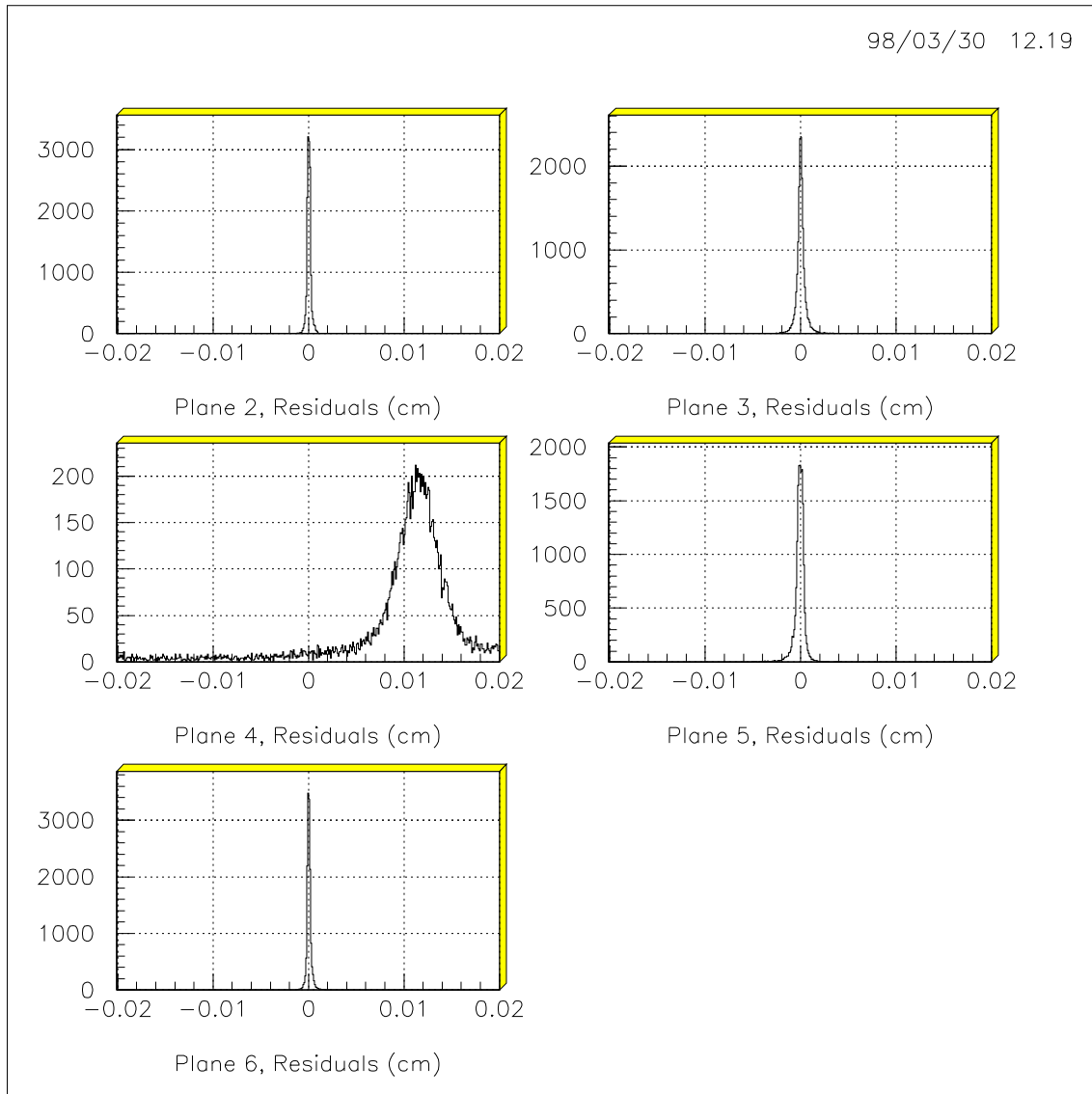


Figure 12: Tracking residuals for each of the five X planes, computed from data acquired at 1850 V with a chamber orientation of 0^0 . The plots were obtained before the appropriate shift of plane 4 was introduced in the analysis.

calculated in three bins in y . If the x-shift of plane 4 was a result of a rotation, the tracking residuals of each y -bin would show a different x-shift; this was not the case. The shift in the tracking residuals of plane 4 was, therefore, mainly a result of an x-shift and not a rotation.

5.5 Tracking Method When Multiple TDC hits are Present

For data acquired with the new front end, about 30% of the TDC channels have multiple hits as shown in figure 4. It is, therefore, important to find out which of these hits should be used for tracking. Since the distance of closest approach of the traversing particle to the sense wire is the one required for tracking (when the drift-circle tangent method is used), the first arrived TDC hit is likely to be the correct one. However, it may happen that the first hit is a result of noise. It is therefore necessary to develop a method that allows us to find the correct TDC hit. To achieve this purpose the tracking code tries all possible TDC hit combinations to construct a track, then chooses the track with the best average tracking residual. About 90% of the time the TDC hit chosen is indeed the one that arrived first.

The average number of TDC combinations per track for run 170 (0° , new front end and 140 mV threshold), is ~ 4 . This number increases for non-zero degree runs as the track intersects more cells. At 60° (run 177 new front end and 140 mV threshold), the average number of combinations is ~ 18 . A simple example might clarify the reason for the non-linear increase in this average as a function of the total number of hits. If a particle passes through the chamber at 0° firing 1 cell/plane (a total of 5 cells) and resulting in two TDC channel hits per cell, the possible number of TDC hit combinations for this track is $2^5 = 32$. If a particle passes through the chamber at some other angle firing 2 wires/plane (10 cells) resulting also in 2 TDC channel hits per cell, the total number of possible hit combinations is $2^{10} = 1024!$

Since trying all possible TDC hit combinations is a CPU intensive process, when a high degree of accuracy is not required, it is convenient to make the assumption that the first arrived TDC hit is the correct one (for example for online analysis). A switch was therefore introduced in the software to allow choosing the first arrived hit or trying all possible combinations.

5.6 Tracking Method When Cross Talk Hits are Present

Dealing with the cross talk hits is a more complicated issue that requires further investigation. While we do expect to be able to reduce the level of cross talk in the next run, a small percentage of cross talk hits will always be present. This is particularly true if we run at a low front end threshold, which will be required to achieve high efficiencies. The following method was therefore developed to allow characterizing and eliminating the cross talk hits.

The method starts by including up to a certain number of plane hit multiplicity (for example three). When more than one wire per plane has fired, it is possible (or even likely for tracks close to zero degrees) that some of these hits are due to cross talk. The tracking code starts by calculating the drift radius for all these hits and uses them all to construct a track. **If the cross talk ratio is small**, the track will be mainly defined by the real hits (as their drift distances are quite consistent with a track), while the cross talk hits are likely to be farther away from the track. The tracking residuals, therefore, provide a convenient handle. A series of cuts are introduced within the tracking iteration process (see section 5.1), starting with a very loose cut on the tracking residuals, re-fitting to adjust the track after the first few cross talk hits are removed (if any), recalculating the tracking residuals, imposing a slightly tighter cut, and repeating the same process again. A six-level cut is currently in the tracking code for this purpose. In addition since the chamber resolutions are a strong function of drift radius (see figure 9), it is necessary to have different cuts depending on drift radius. Three different six-level cuts are therefore used depending on drift radius.

The number of these cuts and their values have not been fully investigated yet. To provide the best possible way for rejecting the cross talk hits several tests will be necessary. It is also important to make a balance between rejecting the cross talk hits while keeping the number of good hits lost by this cut to a minimum. Tests of this method so far do indicate that the method will be effective in removing the cross talk hits.

6 Efficiency

6.1 High Voltage and Threshold Dependence

The efficiency calculation code uses the tracking information to determine which wire cells in the measured chamber should display a hit. If a hit is found, a counter, N_p , for that plane is incremented, where p is the plane number. The efficiency is then defined as

$\epsilon_p = N_p/N_{tp}$, where N_{tp} is the number of times a track is expected to have passed through plane p . In addition to the cuts described in section 5.6 a cut was introduced requiring the average tracking residual to be $< 100\mu m$.

Figure 13 shows the efficiency of the five PDC X planes at high voltages ranging from 1850 V to 2100 V. The efficiency varies significantly with high voltage in this range as well as front end threshold. The particular choice of high voltage and front end threshold, however, will require a balance between efficiency and noise/cross talk. As the high voltage is increased, the efficiency improves, but more noise and cross talk is introduced. Similarly, while lowering the threshold also helps to improve the efficiency, more noise and cross talk is introduced by doing that. The conclusion regarding the best choice of front end threshold and high voltage, therefore, requires a careful examination of the noise and cross talk level which is discussed in the next section.

6.2 Drift Distance Dependence

One of the important decisions required regarding the final chamber design is whether field wires are required. Installing field wires introduces disadvantages in terms of chamber construction and stability, as well as increasing multiple scattering in the chamber. The no-field wire option is, therefore, desired based on this criteria.

The lack of field wires, however, results in a weak electric field region away from the sense wires (zero at the midpoint between any two sense wires), and hits may therefore be lost due to poor electron collection from this region. This weak field region raises a concern about the chamber efficiency as a function of distance from the sense wire. To examine this effect the efficiency was calculated as a function of distance from the sense wire for 0° runs resulting in figure 14. As expected, the lower threshold runs (of 140 mV) provides the best result, since signals arriving from the weak field region are expected to be small and are, therefore, the most likely to be cut out by a high threshold.

6.3 Wire to Wire Variations

Figure 15 shows the efficiency for each cell in the chamber. Variations in efficiency from cell to cell are significant, and tend to show up in certain regions of the chamber. While this might indicate a gas circulation problem, it is also true that chambers 3 and 5 which show lower efficiency for wire numbers < 40 , have also shown much more noise/cross talk at higher voltages than the other planes. In either case, the fact that some regions of the chamber result in high efficiencies indicates that the overall intrinsic efficiency of the

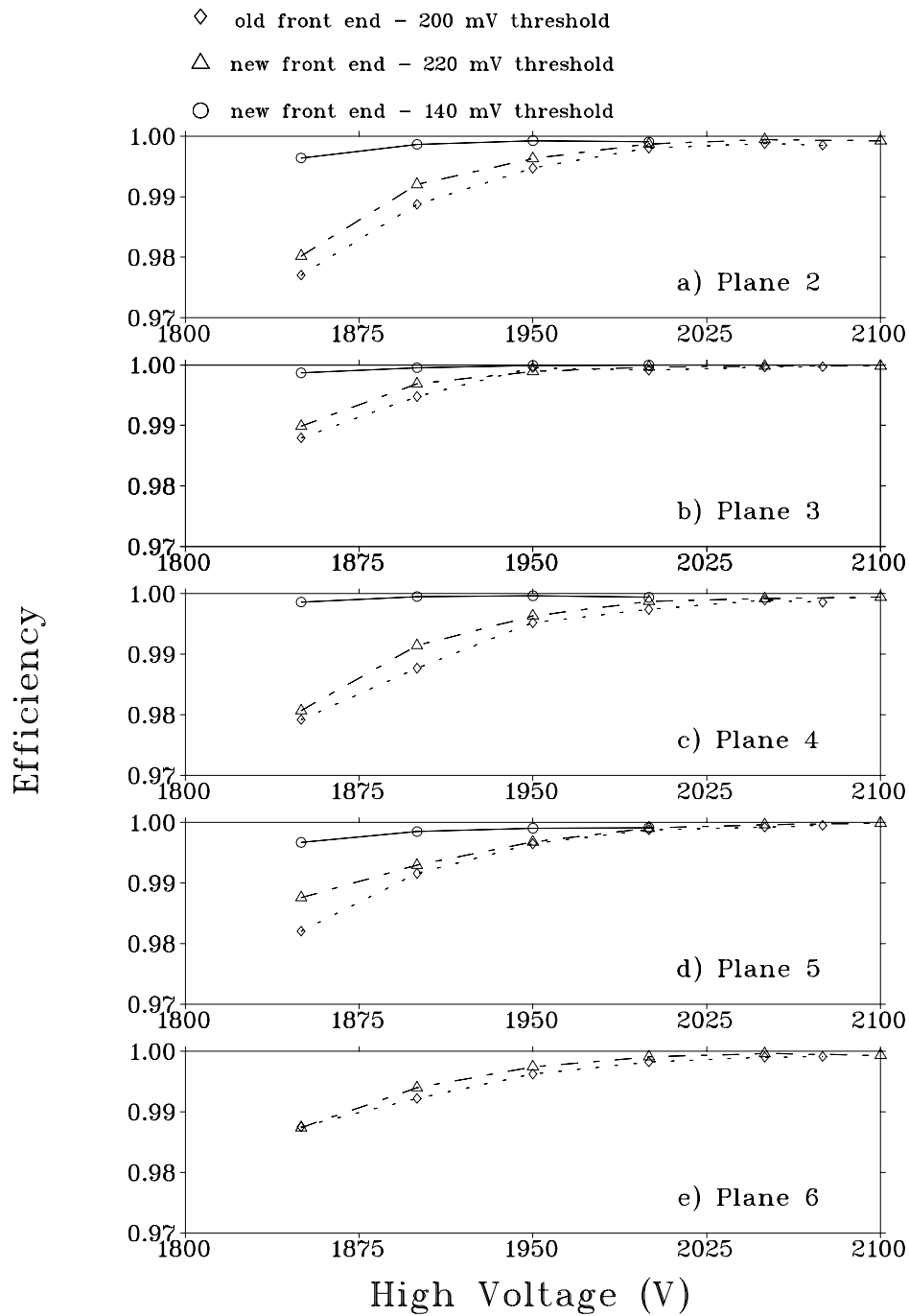


Figure 13: Efficiency as a function of high voltage for the five X planes for data acquired with the old front end at a 220 mV threshold (diamonds), the new front end at a threshold of 220 mV (triangles) and 140 mV (circles).

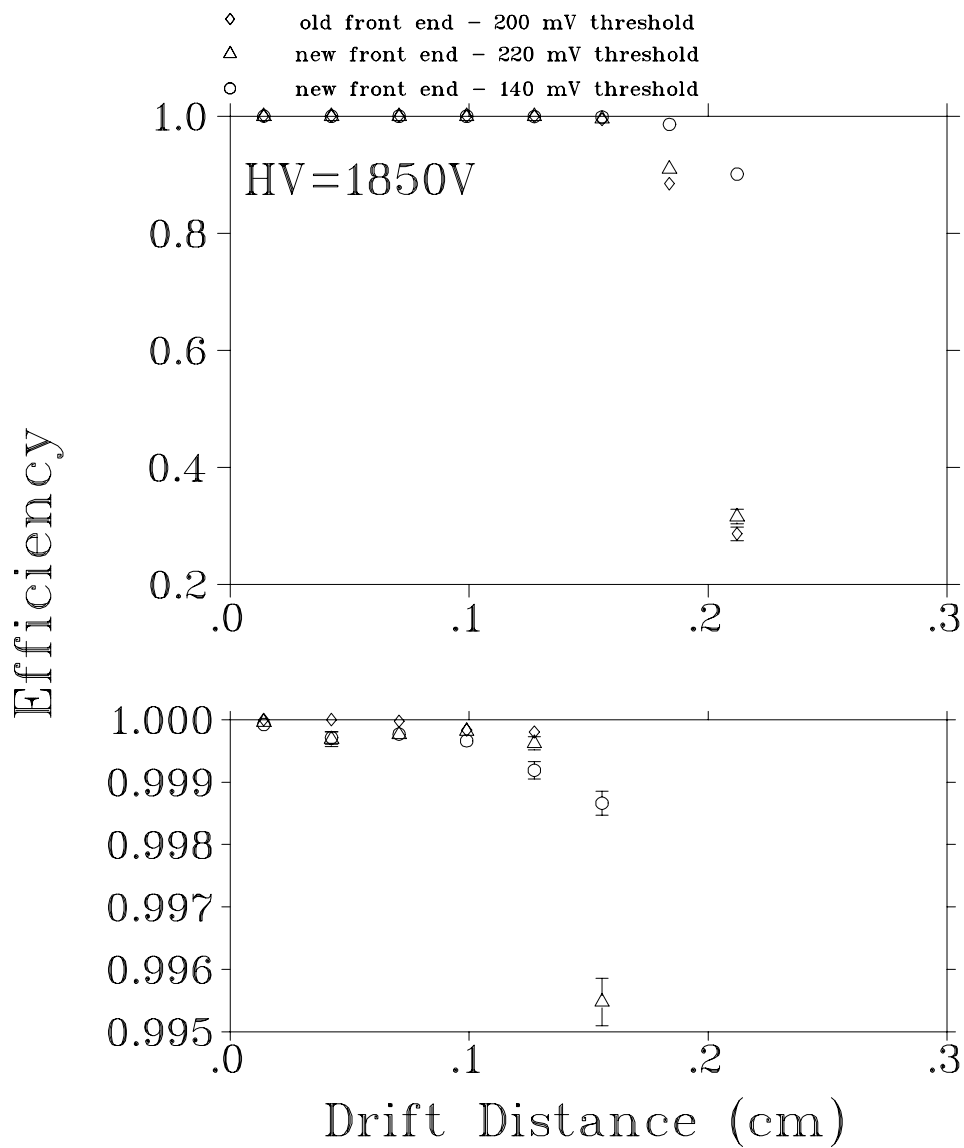


Figure 14: Chamber cell efficiency as a function of distance from the sense wire for data acquired at 1850 V with a) the old front end at a front end threshold of 200 mV (diamonds) b) the new front end at a threshold of 200 mV, and c) the new front end at a threshold of 140 mV. The bottom histogram is a zoomed in copy of the top.

chamber is higher than what is shown in figures 13 and 14, since these figures are summed over all cells.

6.4 Intensity Dependence

All runs at a 140 mV front end threshold were performed at the same beam flux of 500 Hz. We, therefore, have no measurement of the efficiency as a function of intensity. A high level of noise and cross talk (among many other disadvantages) will result in more dead time and might limit our ability to run at a higher flux. Similarly, gas recovery time might result in a lower efficiency. **A measurement of the efficiency as a function of intensity at the proper threshold and high voltage will be necessary to determine the highest beam flux rate that can be tolerated by the E614 chamber.**

7 Noise and Cross Talk

The multiplicity of hits per plane (which results from both cross talk and noise) increases as a function of high voltage. Figure 16 shows the number of events with more than 1 hit/plane as a function of high voltage. All histograms shown in this section are for raw data, no cuts have been applied.

7.1 Noise

During this run, very high levels of noise were observed during the run as well as in the data analysis. Investigation of the test chamber has shown that it was not properly grounded. It was also pointed out that other experiments at TRIUMF had noise problems.

The noise level increases significantly with high voltage. While the TDC spectra at 1850 V are reasonably clean, as the high voltage is increased, multiple peaks start appearing in the TDC spectra of some wires, with the number of wires showing this behavior also increasing with high voltage. Figure 17 shows a couple of these wires in planes 3 and 4 for data acquired at a high voltage of 2100 V and a 220 mV front end threshold. The effect, however, is not restricted to these planes. The frequency at which the noise appears in the spectra is possibly related to the beam bursts. It is worth noting that the TDC spectra for run 170, acquired at a high voltage of 1850 V and a front end threshold of 140 mV, are similar to those acquired at the same high voltage but at a 220 mV threshold.

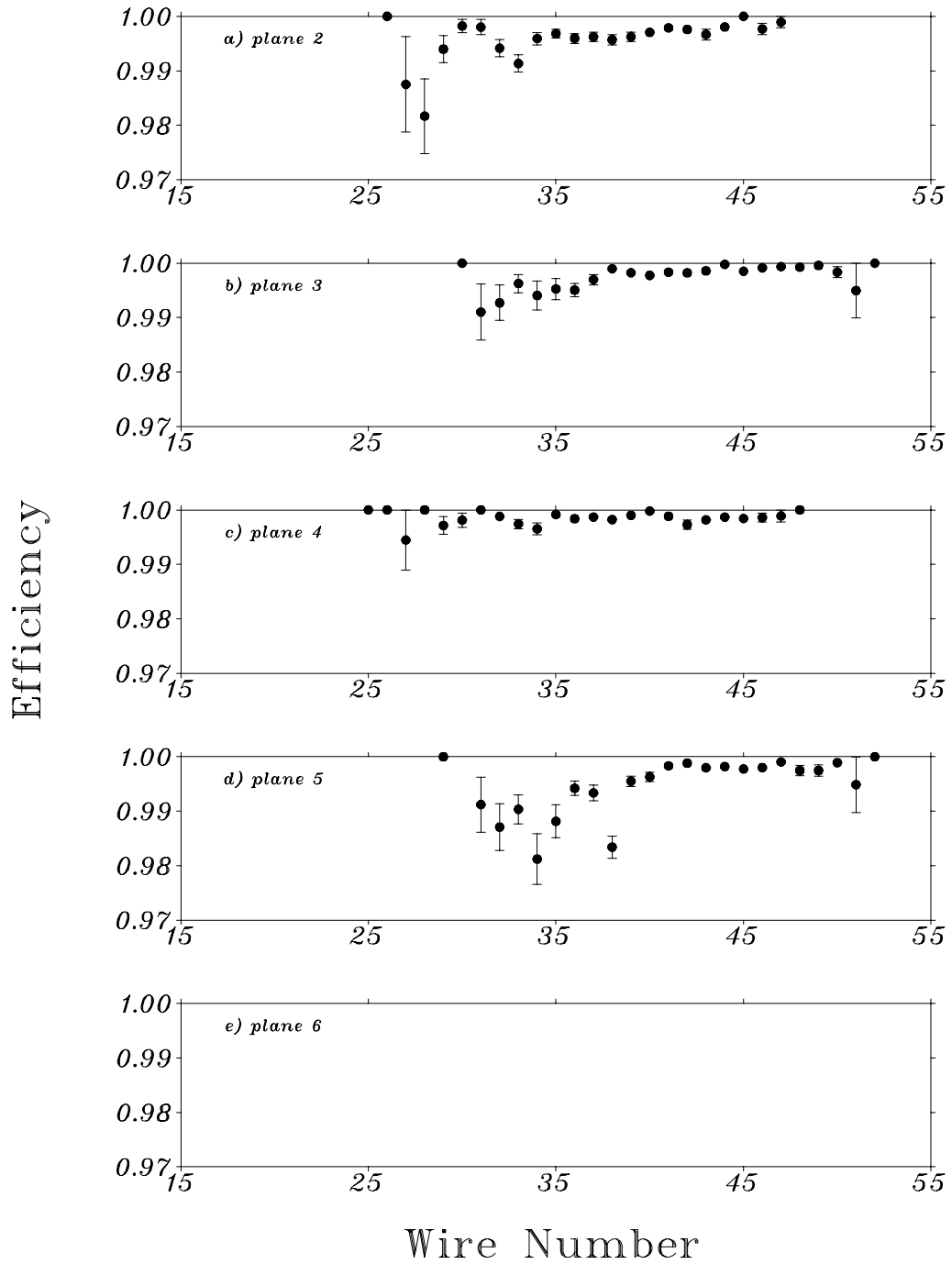


Figure 15: Cell efficiency for each cell in the five X plane.

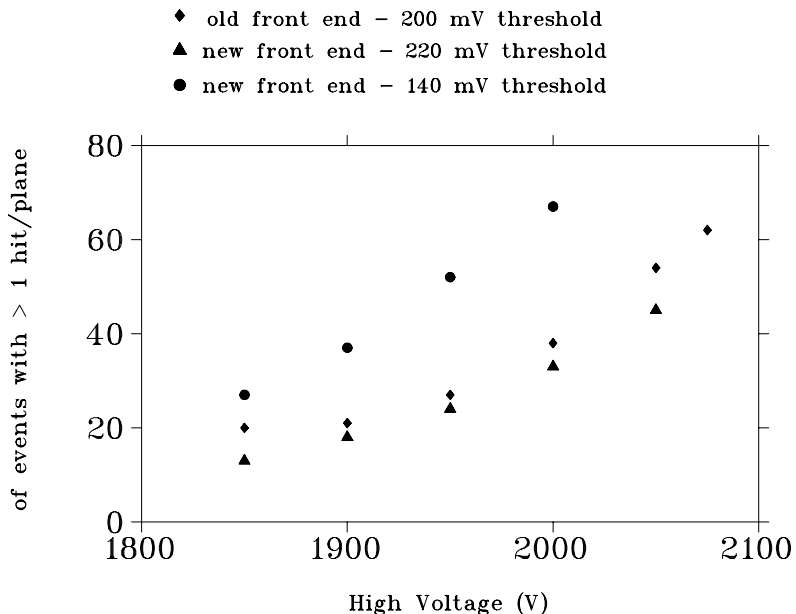


Figure 16: Percentage of events with more than 1 wire firing per plane as a function of high voltage for runs obtained with the old front end at a 200 mV threshold, and the new front end at thresholds of 220 mV and 140 mV. The chamber orientation was 60° for all runs.

7.2 Cross Talk for Minimum Ionizing Particles

The π beam delivered by the M13 channel was chosen to have a momentum of 150 MeV/c, and was therefore minimum ionizing. The cross talk level from the pion beam has a strong dependence on high voltage. Figure 18 shows the number of hits per plane vs plane number for two runs, the first performed at 1850 V (run 159) and the second performed at 2100 V (run 164), corresponding to the left and the right histograms, respectively. It is also worth noting, that the plane hit multiplicity is much higher in planes 3 and 5 than the other planes. While most of the multiple plane hits are due to noise, a good fraction of the 2 and 3 hits/plane tend to be in adjacent wires, as is shown in figure 19, indicating that they are a result of cross talk.

7.3 Cross Talk for Highly Ionizing Particles

Figure 20 shows the multiplicity of hits per plane for all planes at a high voltage of 1850 V, and the wire-to-wire correlation when 2 or 3 wires fire in the same plane. While the cross talk level for the μ runs is much higher than the π runs (which is not surprising since

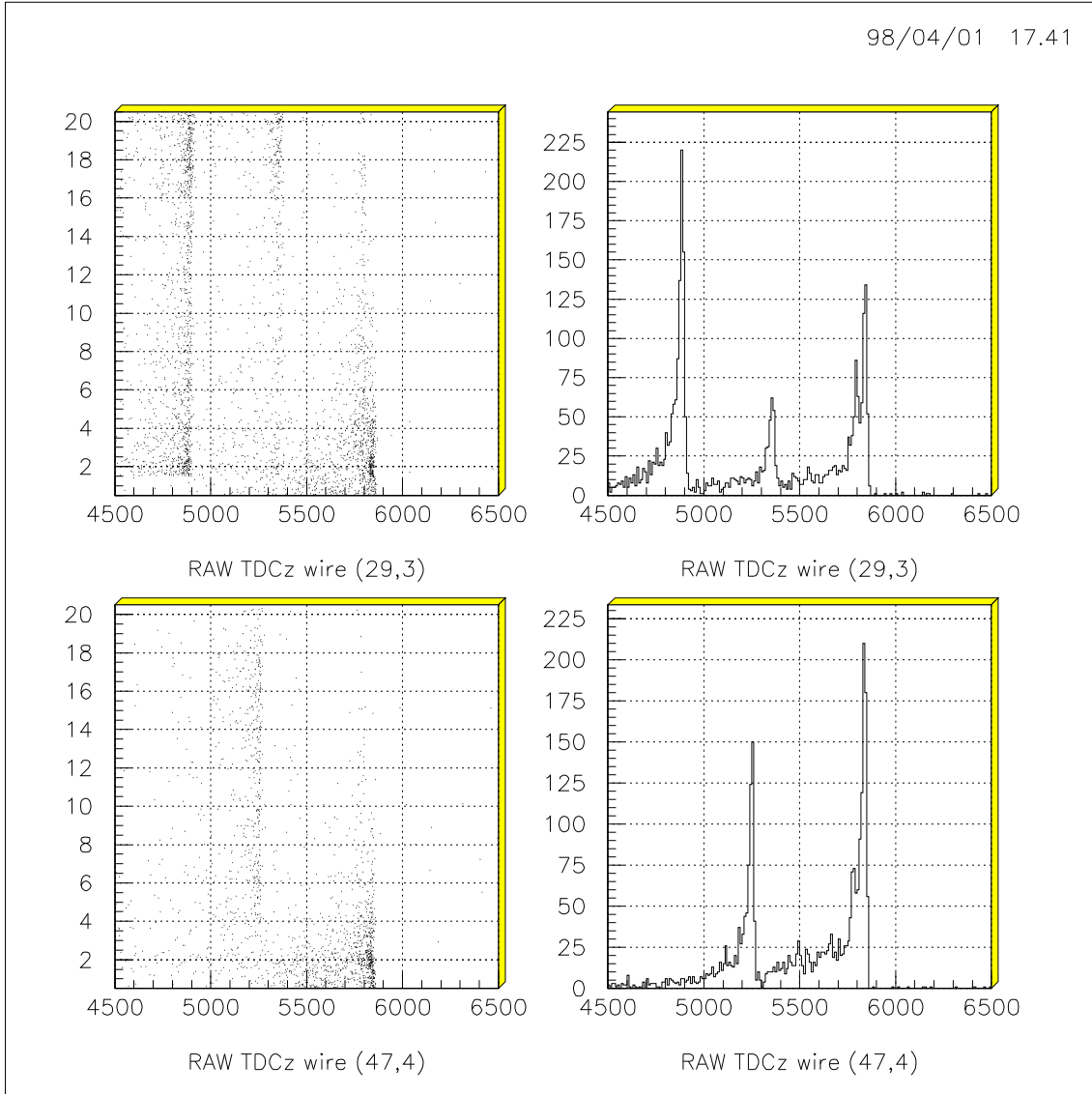


Figure 17: The left histograms are the number of hit wires per plane vs TDC time for wires 29 and 47 in planes 3 and 4, respectively. The right histograms are the TDC spectra for the same wires.

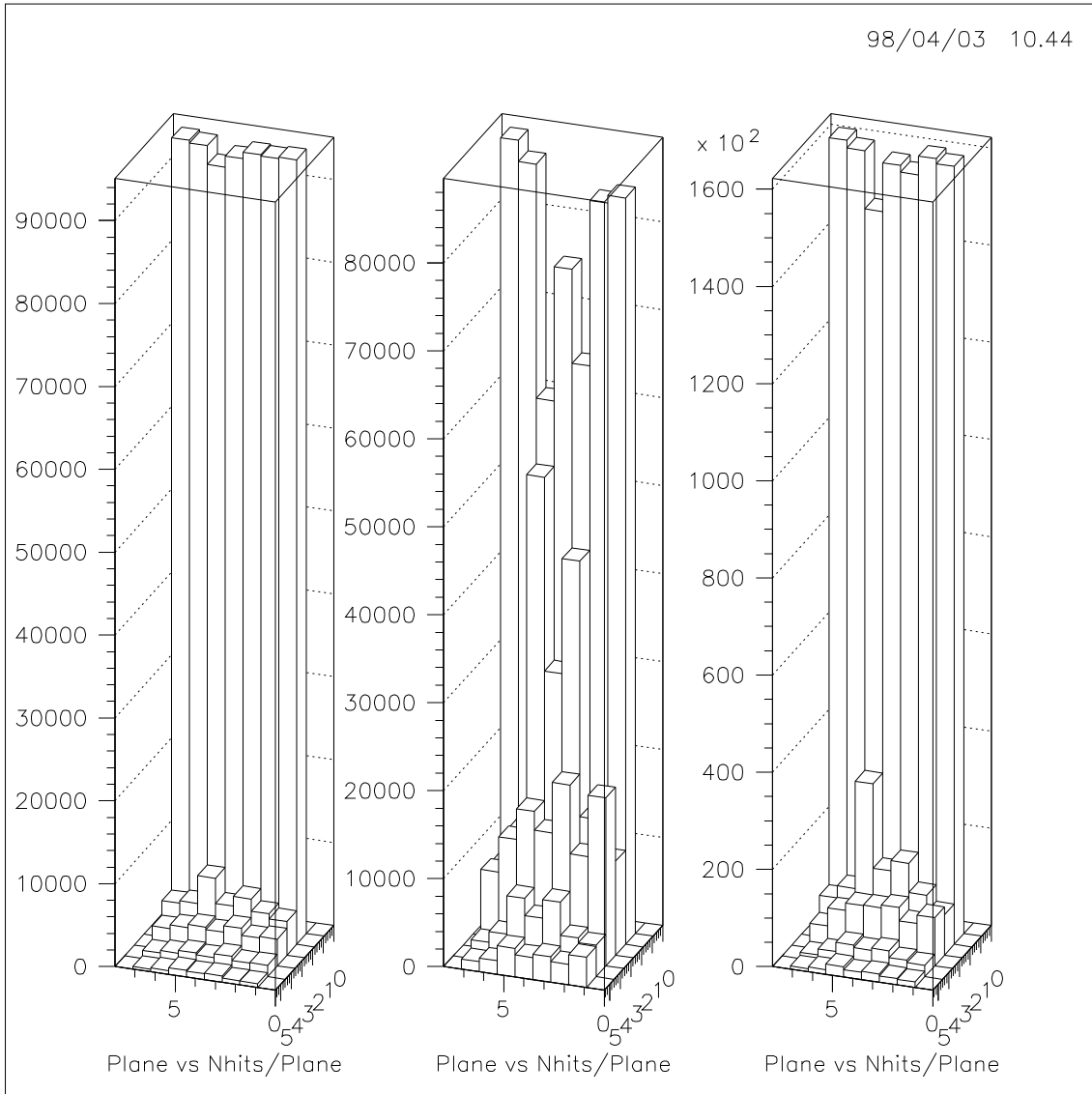


Figure 18: Number of hit wires per plane vs plane number for data acquired with the new front end a) at a 220 mV threshold and 1850 V (left histogram) b) 220 mV threshold and 2100 V (middle histogram), and c) 140 mV threshold and 1850 V (right histogram). All data is acquired with a π -beam.

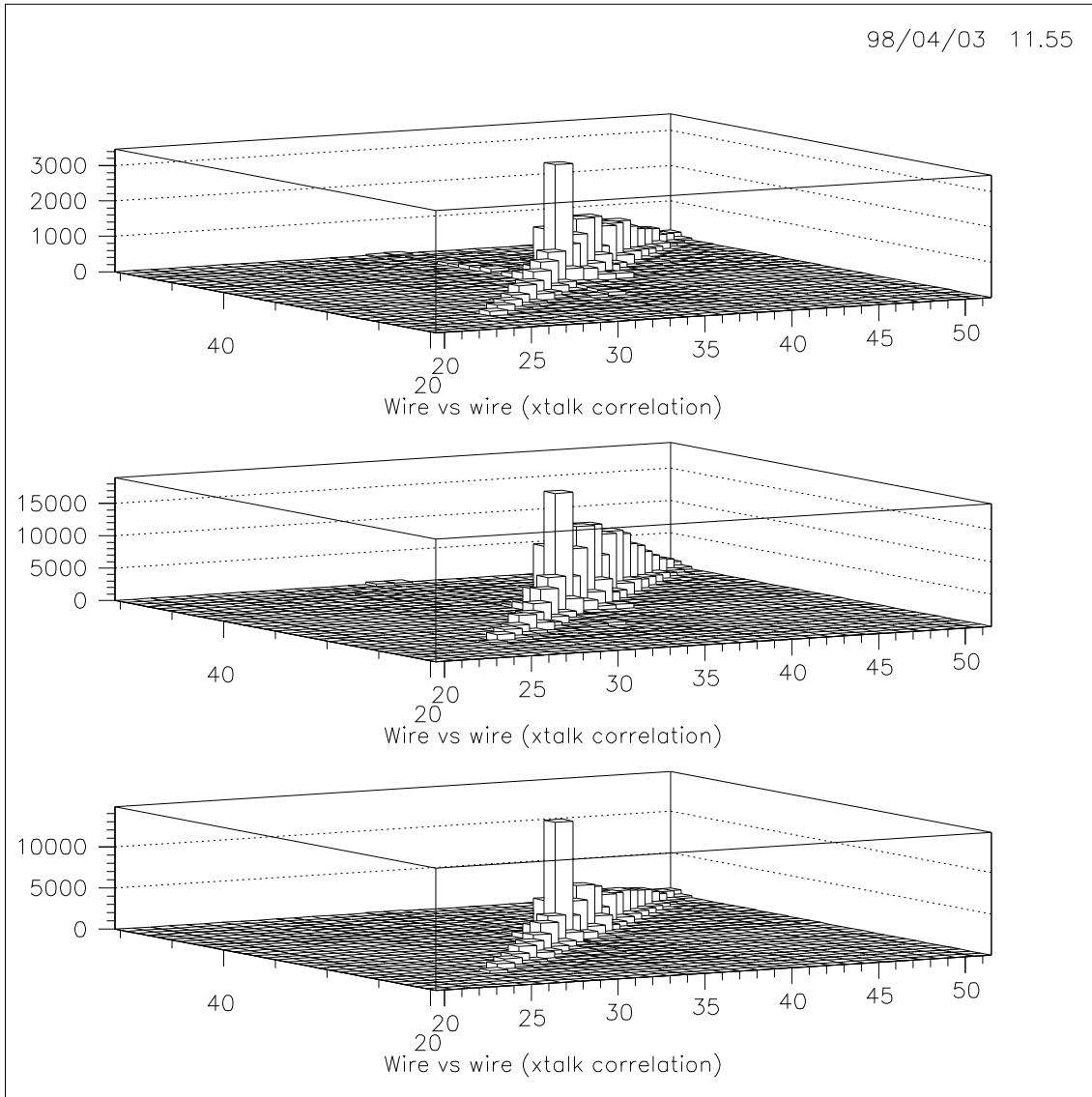


Figure 19: Wire number for a hit wire vs wire number for another hit wire in the same plane when 2 or 3 wires fire in that plane. All histograms are for data acquired with the new front end. The top two histograms are for data acquired 220 mV threshold and a high voltage of 1800 V and 2100 V, respectively. The bottom plot is for data acquired at a 140 mV threshold and 1850 V. The histograms show that when 2 or 3 wires fire in one plane they are likely to be adjacent, indicating cross talk.

they are highly ionizing), in general, only one or two wires adjacent to the muon track fire. This result is quite encouraging as it shows that the muon beam passing through the E614 chamber will not result in dead times over a wide range of the chamber.

Increasing the high voltage results in a substantial increase in cross talk. Figure 21 shows the number of wires firing per plane at high voltages of 1800 V, 1850 V, and 1900 V. There is a considerable advantage in running the chamber at lower voltage.

8 Improved Calibrations

The following is a suggested method for an accurate calibration of the chamber. The best way to proceed with the calibration is to start by obtaining a GARFIELD calibration file where all the parameters are supplied to GARFIELD properly. In this case the calibration file should be accurate enough (hopefully below $50 \mu m$) to start with for finding TDC time zero T_0 and the wire positions (x_w, z_w) to a comparable accuracy.

8.1 Finding TDC Time Zero

The tracking residuals should be calculated such that a residual is negative when a track passes inside a drift circle, and positive when it passes outside a drift circle. The average tracking residual for a given wire will then give information about whether the value of T_0 is lower or higher than it should be. An iteration over T_0 should be done until the value of the average tracking residual for each wire is close to zero.

8.2 Finding the Wire Positions

For each wire the position (x_w, z_w) need to be found. The data acquired with a chamber orientation of 0° is useful to un-couple x_w from z_w . Once x_w is determined for all the wires from 0° runs, the high angle runs may be used to obtain z_w .

To find the wire positions, the tracking residuals should be calculated such that a residual is negative when the track passes to the left of the wire, and positive when it passes to the right of the wire. The average tracking residual for a given wire will then give information about whether the actual wire position is to the left or to the right of where it should be. An iteration over x_w and z_w should be done until the value of the average tracking residual for each wire is close to zero.

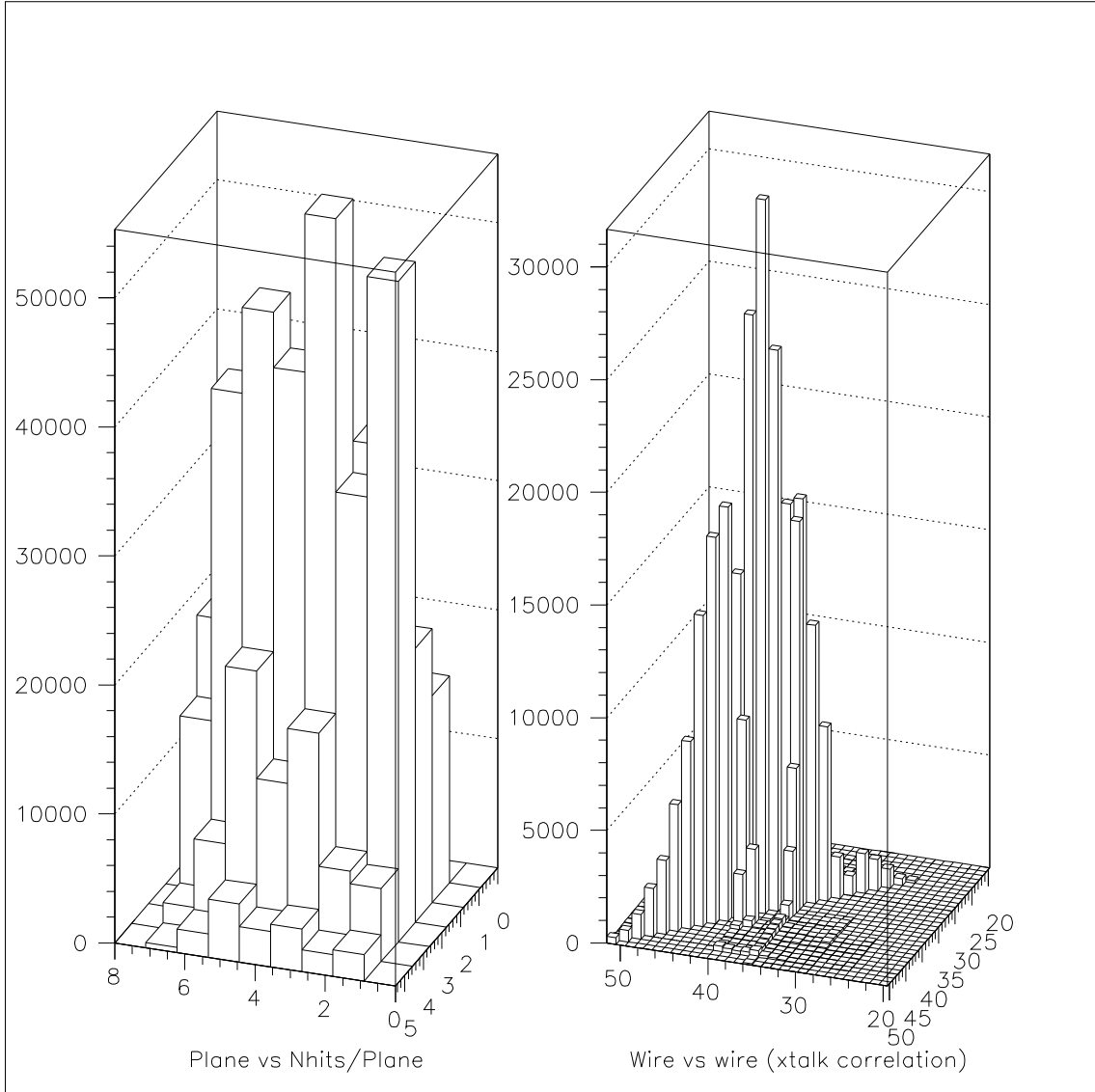


Figure 20: **Left:**Number of hit wires per plane vs plane number. **Right:** Wire number for a hit wire vs wire number for another hit wire in the same plane when 2 or 3 wires fire in that plane. The histograms are for μ -beam data acquired with the new front end at a high voltage of 1850 V.

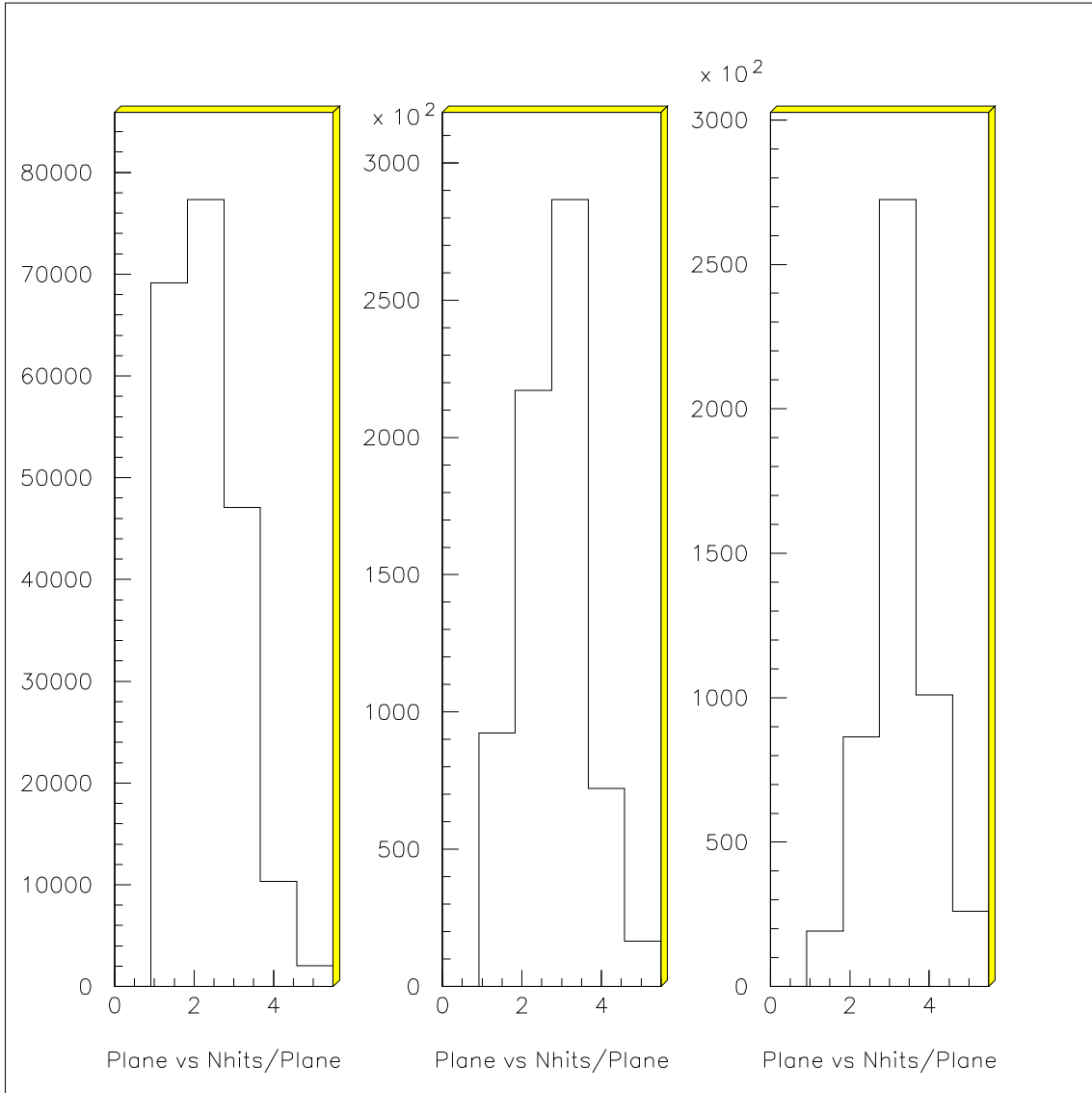


Figure 21: **Top:**Number of hit wires per plane vs plane number projected on the y-axis (i.e. number of hit wires per plane summed over all planes) at a high voltage of 1800 V (left), 1850 V (center), and 1900 V (right). All data is for muons acquired with the new front end.

8.3 Fine Tuning the GARFIELD File

If we decide that fine tuning the GARFIELD file is necessary to obtain the resolutions required, a method similar to the calculation of T_0 may be used with the only difference being that the average tracking residual should be calculated for each TDC channel (or group of channels). A negative (positive) average tracking residual for a given channel implies that the drift distance R_d corresponding to a given TDC channel is lower (higher) than it should be, and an iteration is required to bring the value of these averages to zero.

8.4 The BIG Iteration

Since all the above parameters (T_0 , x_w , z_w , and $R_d(\theta_t, t)$) are interdependent, an overall iteration needs to be done, so that the above steps are repeated enough times for this process to converge.

9 Conclusions

The test chambers have demonstrated both a good efficiency and resolution. The high level of noise and cross talk, however, is a reason for concern. **Serious work has to be devoted to reducing the noise and cross talk.** If the noise and cross talk remain at their levels in this test run, the chamber would have to be operated at a high voltage in the range of 1800-1900 V and a front end threshold of 100-150 mV to achieve high efficiency (of about 99.8% at 0°) while keeping the noise and cross talk at tolerable levels. If the noise and cross talk levels are substantially improved, it will be possible to run at a higher voltage, therefore, achieving a higher efficiency.

While the efficiency near the edge of a cell drops significantly as a result of the lack of field wires, this data shows that a proper combination of high voltage and front end threshold can limit this drop, so that the overall efficiency of the cell remains high. A significant decrease in noise and cross talk will allow us to run at a higher voltage, which results in strengthening the field near the cell edge and, therefore, further reduce the drop in efficiency.

The narrow widths of the tracking residuals (summed over all wires in each plane) reflects a good accuracy in the wire positions. The individual planes, however, were not well aligned with each other, and a shift parameter had to be introduced for each plane. It is critical that a good plane-to-plane alignment is achieved, as well as accurate wire positioning.

The chamber resolution is summarized in figure 9. The efficiency results are summarized in figures 13. Noise and cross talk results are summarized in figure 16.